Cellulose (2023) 30:6487–6505
https://doi.org/10.1007/s10570-023-05267-9

ORIGINAL RESEARCH

Electrospun manuka honey@PVP nanofibers enclosing chitosan-titanate for highly effective wound healing

Lamyaa M. Kassem · Ahmed G. El-Deen · A. H. Zaki · S. I. El-Dek

Received: 23 July 2022 / Accepted: 14 May 2023 / Published online: 6 June 2023

Abstract The major challenge in skin tissue engineering is the creation of physically and functionally suitable extracellular matrix (ECM) scaffolds. A manuka honey-treated polyvinyl pyrrolidine (Mh@PVP) composite was successfully electrospun to produce nanofibrous scaffold that aids in the rapid growth of ECM and serves as a vehicle for drug delivery. Different characterizations namely SEM, XRD, and FTIR were utilized to elucidate the fabricated electrospun nanofibrous scaffolds (ENS). By increasing the concentration of manuka honey (Mh) in the formula, the mechanical, tensile, and conductivity properties of the polyvinyl pyrrolidine (PVP) solutions were significantly improved. As the concentration of honey rose, the width and direction of the ENS produced altered. For wound healing, honey's ability to heal wounds faster may be boosted by a higher PVP concentration, which makes honey more easily incorporated. Because of its burst-and-continuous methylglyoxal release patterns, which may last for up to seven days, Mh is an excellent choice for helping the body's healing process. The in vivo assessment of the Mh@PVP nanocomposite nanofiber mat demonstrated a rapid and substantial increase in keratinocyte expression, reflecting great ability for high regenerative wound healing. Most significantly, there is no scarring associated with hair regrowth. This scaffold can mimic skin characteristics and stimulate keratinocyte development.

L. M. Kassem · A. H. Zaki · S. I. El-Dek (✉)
Materials Science and Nanotechnology Department,
Faculty of Postgraduate Studies for Advanced Sciences,
Beni-Suef University, Beni-Suef 62511, Egypt
e-mail: samaa@psas.bsu.edu.eg

L. M. Kassem
e-mail: Lamyaa.ucp@gmail.com

A. H. Zaki
e-mail: ayman.zaki@psas.bsu.edu.eg

A. G. El-Deen (✉)
Renewable Energy Science and Engineering Department,
Faculty of Postgraduate Studies for Advanced Sciences,
Beni-Suef University, Beni-Suef 62511, Egypt
e-mail: ag.eldeen@psas.bsu.edu.eg

Graphical abstract

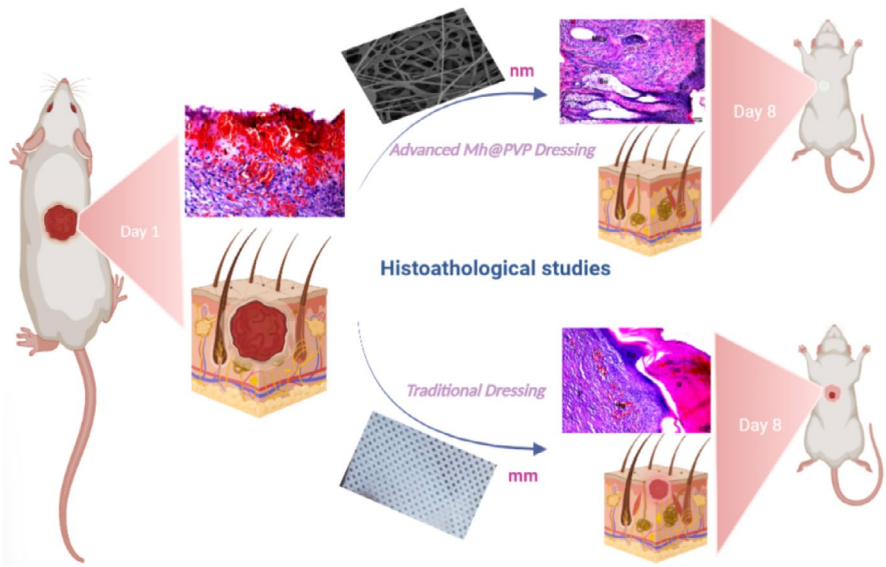

Keywords Manuka honey · PVP · Chitosan titanate · Nanofibers · Wound healing and dressing · Electrospinning

Introduction

Electrospinning is gaining popularity as a novel technique for production of natural and/or synthetic polymer driven nanofibers. fabrication of advanced wound dressing through electrospun nanofibers offers the potential to fit with the current trend and pharmaceutical market needs for unique pharmaceutical products with controlled and targeted drug administration. Multiple researches were conducted in this field and the challenge always is the selection of the polymer and to study the ability to be loaded with medicine. This advanced dressing can help to treat acute wound after surgery or trauma as well as chronic wounds as diabetic foot and bed sores offering good healing properties and cost-effective manner opportunities. (Jeckson et al. 2021; Liu et al. 2021; Rajput et al. 2021; Pavan Kalyan and Kumar 2022). Fabrication of dressing of biodegradable and biocompatible polymer that helps high quality of healing with low cost and with decreased possibility of adverse effects and complications was the main aim of this study. To successfully manufacture an electrospun wound dressing, it is necessary to optimize the process, make appropriate polymer selections, and conduct several characterization studies (Ahmed and Xu 2020; Augustine et al. 2020). Polyvinyl pyrrolidine (PVP) is a biocompatible, biodegradable synthetic polymer that is frequently combined with other natural and/or synthetic polymers to fabricate a variety of wound dressings; it assists in the formation of the healing mesh and absorbs wound exudate (Zahedi et al. 2010; Aytimur and Uslu 2014; Alipour et al. 2019; Shitole et al. 2020; Contardi et al. 2021). Owing to the growth of drug-resistant germs, honey has recently re-emerged as a therapy for chronic and deep ulcerations. The antibacterial and therapeutic properties of honey are influenced by the type and amount used. Manuka honey (Mh) is a rare variety of honey made from the nectar of the Leptospermum scoparium tree native to New Zealand(Adams et al. 2009; McDonald et al. 2018). Mh inhibits inflammatory cell production and proliferation, allowing normal wound healing and stimulating fibroblast and epithelial cell growth. Moore concluded after reviewing a large body of literature that Manuka honey possesses extraordinary therapeutic properties and is the world's greatest natural antibiotic (Moore et al. 2001; Maddocks et al. 2012; Patel and Cichello 2013; Bogdanov 2015;

Georgescu et al. 2017). Mh's antibacterial properties are non-peroxide based, owing to its high methylglyoxal (MGO) content. Heating of manuka honey at a moderate temperature (50 °C) modifies the crystallinity and chemical composition of its constituents that negatively impact the nutrient activity of honey and thus affecting its healing enhancement and antibacterial properties, the Mh may change into caramel, MGO creates a covalent link with the amines in the honey matrix (Siti Sarah 2016). Crosslinking conditions must be optimized because heating of Mh@PVP ENS may adversely influence the nanoscale property of the electrospun nanofibers. During heating, (Atrott et al. 2012; Kato et al. 2021). Mh contains a high concentration of sugars, free amino acids, proteins, enzymes, essential minerals, vitamins, and secondary metabolites (flavonoids, phenolic acids, and 1,2-dicarbonyl compounds). It is currently being used as an alternative remedy for bacterial, fungal, parasitic, and viral infections in a large number of patents (Gethin et al. 2008; Molan and Rhodes 2015; Yilmaz and Aygin 2020). Manuka honey keeps wounds moist and acts as an autolytic debriding agent. Several clinical trials and in vivo bacterial challenges have proven manuka honey's broad-spectrum antibacterial efficacy (Gethin and Cowman 2005, 2008; Majtan 2011; Rafter et al. 2017; El-Senduny et al. 2021). Additionally, laboratory studies have demonstrated that manuka honey has an effect on the molecular structure of a variety of bacteria (Badet and Quero 2011), namely, *Methicillin-resistan Staphylococcus aureus* (MRSA) (Cooper et al. 2002; Henriques et al. 2010), *Pseudomonas aeruginosa* (Henriques et al. 2011; Roberts et al. 2012), *Escherichia coli* (Blair et al. 2009) and *Streptococcus pyogenes* (Cooper et al. 2011). Manuka honey has antioxidant and anti-inflammatory properties that promote the healing process (Deng et al. 2018; Stagos et al. 2018; Ronsisvalle et al. 2019; Pentoś et al. 2020). Electrospinning pure honey into nanofibers is a tricky task, owing to honey's hygroscopicity and low viscosity (Sarhan et al. 2016). Cospinning manuka honey with other easily spun polymers, such as PVP, is the most effective way to overcome this limitation. Titanate nanotubes (TiONTs), hollow and multiwalled nanostructure with a high aspect ratio (Pandey et al. 2019; Ranjous et al. 2019; Xiao et al. 2020; Baati et al. 2021; Boudon et al. 2021). TiONTs was investigated as a possible carrier for pharmaceutical active ingredients and for the development of novel dosage forms that address several of the pharmaceutical industry's challenges, including cytotoxic chemotherapy drug delivery, targeted drug delivery to the brain and bone, and controlled release of medications such as Diltiazem hydrochloride, diclofenac sodium, atenolol, and hydrochlorothiazide and it also used to counter against antibiotic resistance (Sipos et al. 2017; Ozkizilcik et al. 2018; Jose et al. 2020; Razak et al. 2021; El Nahrawy et al. 2021; Sandomierski et al. 2022). Titanate nanotubes generated hydrothermally have limited utility for nanovectorization systems due to their low suspension stability, high aggregation ability, and chemical inertness toward biological systems. Modification of the surface of TiONts (grafting) with biocompatible compounds appears to be a viable strategy for circumventing these constraints. Few studies have been conducted to investigate the use of TiONts surface grafting in biomedical applications (Pan et al. 2015; Sallem et al. 2017). Chitosan is a polyelectrolyte with unique physicochemical and biological properties, such as biocompatibility, antibacterial activity, and biodegradability into non-toxic chemicals. Chitosan's positive charge is required for cell interaction because it increases the efficacy of gene transfer, medication administration, and imaging, but it also increases the risk of cytotoxicity (Matica et al. 2019; Cavallaro et al. 2021; Seidi et al. 2021, b; Shoueir et al. 2021; Wani et al. 2021). Titanate grafting with chitosan improves the solution stability of titanate and decreases the crystallinity of chitosan, hence limiting the effect of chitosan on drug dissolution from CT-TiONTs and conferring an advantage property on CT-TiONTs nanocarriers (Habiba et al. 2016; Sinaei et al. 2020; Wang et al. 2021). Chitosan coated Titanate can be used to modify drug's bioavailability and pharmacokinetic parameters, such as water/lipids solubility, tissue and bone distribution, and resistance to enzymatic degradation, while keeping its solution stability and bioactivity.

By utilizing a concentrated PVP solution, we developed a novel nanoelectrospun scaffold with a high manuka honey content and a high MGO 500 + to promote a high quality of healing for deep and chronic wounds. The Mh@PVP scaffold was loaded with chitosan-coated titanate to serve as a potential drug delivery nanocarrier. Nonetheless, there is a dearth of published research on polymer integration with Manuka honey. We demonstrate the synthesis,

characterisation, and optimization of the CT-TiONTs loaded Mh@PVP ENS fabrication process using the foregoing knowledge. The effect of a non-medicated Mh@PVP scaffold on wound healing was investigated using rat models, histology, and cytotoxicity.

Methods

Chemicals and methods

All chemicals and reagents used in this study were of analytical quality and did not require additional purification. Sodium hydroxide (NaOH) Piochem for laboratory in Egypt. Hydrochloric acid 32% (HCL) CARLO ERBA Reagents. Glutaraldehyde (C5H8O2) 25% in H_2O, Sigma Aldrich. Glacial acetic acid 99–100% (C2H4O2), Merck. Chitosan (C56H103N9O39) 240 kDa and DDA of 84%, Chitoclear, cg110, Sigma Aldrich. Polyvinylpyrrolidone (C6H9NO) Mwt 9000, 85kDa, 99% hydrolyzed Sigma Aldrich. Manuka honey (UMF18 + /MGO 500) PURITI products, New Zeeland. Glucose Assay Kit, Sigma Aldrich.

Production and Characterization apparatuses

Hand made Electrospinner machine, Faculty of Egnginnering, Minia University, Egypt. The Zetaszer Nano ZS91 was used to determine the surface Zeta potential of the samples using dynamic light scattering analysis (Malvern instruments). Bruker AXS D8 instrument (Cu K), Patterns of X-ray diffraction (XRD). 40 kV and 20 mA were used as the accelerating voltage and applied current, respectively, with a general area detector diffraction system (GADDS), The distance between the detector and the sample for WAXD was 47.0 mm. IR spectra were acquired with a resolution of 4 cm^{-1} in the range 500–4000 cm^{-1}. Bruker FT-IR Tensor 27 spectrophotometer used to ascertain the molecular interaction of PVP, Mh, and CT-TiONTs. Images of electrospun fibers were collected using a field emission gun scanning electron microscope (Philips XL30 FEG). Prior to SEM analysis, the samples were carbon coated using the Edwords coating system E306A. Radelkis OK-102/1 conductivity meter used to meaure the solution conductivity. HAAKE Roto Visco rheometer at 25° C used to measure viscosity. The JQ03B (Powereach, China) micro tensile testing machine was used to conduct tensile tests.

Fabrication of wound dressing scaffold nanofiber composite

Titanate nanoparticles Preparation

Titanate nanoparticles were synthesized using a hydrothermal technique according to the study of Farghali et al. (2016) with small modifications. To prepare TiO_2 nanotubes, 5 g of TiO_2 bulk powder was added to 250 mL of 10 M NaOH aqueous solution while stirring continuously. The solution was then placed in a Teflon-lined stainless-steel autoclave with a 1000 mL capacity and heated at 160 °C for 20 h. The white precipitant was collected and washed with distilled water several times. Ultrasonically washed samples with 0.1N HCl solution, and the precipitates were finally dried at 100 °C for 12 h.

Grafting of chitosan on titanate nanotube surface

Using the solution-casting approach, the CT-TiONTs nanocomposite was produced by mixing two equal portions of 2.5% chitosan and 2.5% TiONTs solutions in acetic acid and stirring for four hours at 80 °C. In order to completely eliminate any residual acetic acid,

Table 1 Morphological summary and diameters of the Mh@PVP ENS

Sample (Composite)	Min. diameter (nm)	Max. diameter (nm)	Average diameter (nm)	Fiber Morphology
A (Mh25%@PVP)	53	1638	368	Heterogenous
B (Mh20%@PVP)	65	582	257	Heterogenous
C (Mh15%@PVP)	210	571	37	Homogenous
D (Mh15%@PVP; 50 °C)	614	1608	1038	Heterogenous
E (Mh15%@PVP; 30 °C)	296	591	397	Homogenous

the resultant suspension was degassed and ultrafiltered (350 kDa, RC) with deionized water multiple times. CT-TiONTs nanocomposite powder was produced by dehydrating the filtered suspension at 35 °C for the next 24 h.

Mh@PVP blend solution preparation

The electrospinning settings were optimized to produce smooth and continuous nanofibrous scaffold. To obtain the optimal healing and antibacterial efficacy of manuka honey, the nanoelectrospun scaffold has to contain the largest amount of honey possible. Using the electrospinning technology to integrate a large percentage of manuka honey is made difficult by the physical properties of honey. This issue could be resolved by increasing the PVP concentration in the blend solution, which allowed the incorporation of a higher percentage of honey with PVP. Therefore, a 15% w/v PVP solution was prepared and mixed with various manuka honey/polyvinyl pyrrolidine solutions at escalating honey concentrations using the following volume percent ratios of manuka honey to polyvinyl pyrrolidine v:v (%); 1:3 (25%), 1:4 (20%), and 3:17 (15%). Both PVP solution and honey are miscible and water soluble. Mh@PVP blends were stirred continuously for 48 h at room temperature until they were homogeneous and completely clear. Following that, the conductivity of the prepared blend solutions was determined using a conductivity meter (Ysi 3200), as detailed in Table 1. Subsequently, using an electrospinner, the aged solutions were electrospun. After electrospinning, the ENS was gently peeled away from the aluminium foil and vacuum dried overnight. During electrospinning, the humidity and temperature were maintained at 30–35% and 24 °C, respectively.

Loading of Mh@PVP blend with CS/TiONTs (CT-TiONTs/Mh@PVP), Fig. 1

Solution casting was used to produce a CT-TiONTs-loaded Mh@PVP composite. CT-TiONTs were dispersed in ethanol by sonification and stirring for 4 h, and then 0.5 g of CT-TiONTs was added to the previously prepared Mh@PVP blended solutions with continuous stirring for 12 h, until a homogenous and clear solution of CT-TiONTs/Mh@PVP was obtained.

Electrospinning process optimization

Using a bi-packed 21G (0.80 × 38–40 mm) needle, a 10 mL plastic syringe was loaded with the prepared Mh@PVP solutions and affixed to the nozzle. By varying the flow rate between 0.5 and 1 mL/h, the applied voltage between 15 and 22 kV, and the fiber collecting distance between 15 and 20 cm, the optimal process conditions for obtaining smooth and continuous fibers were identified. The experiments demonstrated that the following electrospinning parameters produced the best results in terms of fibrous scaffold fabrication: 1 mL/h flow rate, 19 kV applied voltage, and 18 cm collecting distance; all scaffolds were prepared using these settings.

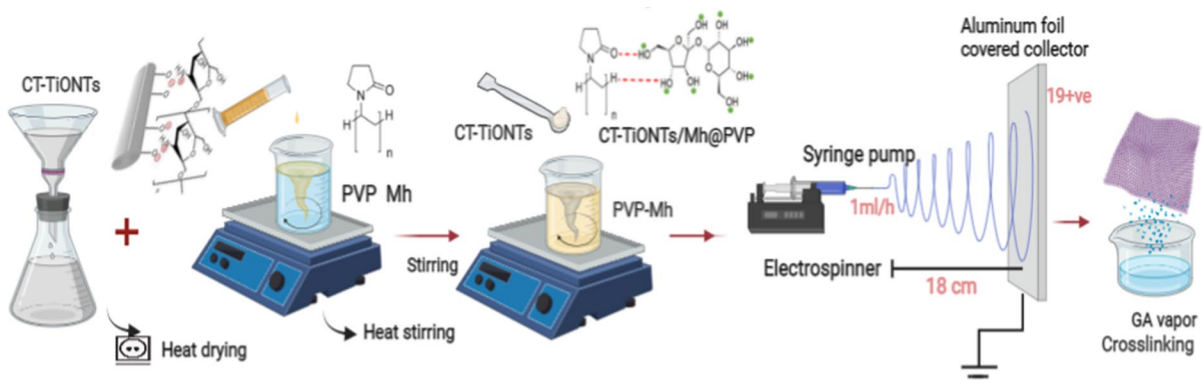

Fig. 1 Electrospinning preparation scheme for a nanofibrous CT-TiONTs/Mh@PVP scaffold

Mh15%@PVP scaffolds with enhanced morphology were the finest (Fig. 3c, e). Secondary branching jets formed at flow rates less than 1 mL/h. These jets were unable to reach the collector because a stable Taylor cone, which is required for fiber synthesis, could not be formed.

Cross-linking of nanofiber scaffolds

Crosslinking enables nanofibrous scaffolds to retain their nanofibrous structure in aqueous environments, thereby increasing porosity and enabling controlled release applications for medicine. However, increasing the degree of crosslinking can reduce the nanofibers' swelling ability due to the network's increased rigidity as a result of increased inter- and intramolecular interactions (Sarhan et al. 2016). While swelling ability is directly related to honey concentration, it is indirectly proportional to crosslinking degree, and therefore both should be optimized to preserve the scaffold's proper swelling ability. The ENS of CT-TiONTs/Mh15%@PVP were cross-linked by exposure to glutaraldehyde (GA) vapours at two different temperatures for 12 h: 30 °C and 50 °C, Fig. 3d and e. Characterization was performed to determine the optimal crosslinking technique, and 12 h of exposure to GA vapour at 30 °C was chosen as the optimal crosslinking condition. Following that, the crosslinked nanofibrous scaffolds were subjected to a fume hood for 5 h to evaporate any remaining glutaraldehyde vapor to reduce the risk of cytotoxicity (Tang et al. 2019). Crosslinking Mh@PVP electrospun nanofiber scaffolds was challenging due to heat sensitivity of honey(Kato et al. 2021), necessitating optimization of the temperature at which the mat is exposed to GA vapours. Honey shouldn't be heated rapidly over direct heat, UV irradiation is a crosslinking approach that was utilized to crosslink variable PVP composites (Morsi et al. 2019; Głąb et al. 2021), but it was not successful in crosslinking Mh@PVP.

Permeability of water vapor (PWV).

The water vapor permeability was determined using the cup test method according to BS 7209 [Standard, 1990 #272], where four samples of PVP and CT-TiONTs/Mh15% @PVP were evaluated and the mean and standard deviation (SD) values were recorded. According to Eqs. (1 and 2), the weight loss was translated to vapor permeability.

$$PWV(g.m-2.day-1)=\frac{24M}{At} \tag{1}$$

$$A=\frac{\pi d2X10-6}{4} \tag{2}$$

where M is the mass loss in grams, t is the duration between weightings in hours, A is the interior area of the dish in square meters, d is the internal diameter of the dish in millimeters, and WVP is the water vapor permeability of the test fabric.

Tensile stress test

The PVP, Mh15%@PVP, Mh20%@PVP, Mh25%@PVP and CT-TiONTs/Mh15%@PVP scaffold's tensile characteristics in dry and wet state were determined. For this investigation, the maximum load in Newtons, the extension at maximum load in millimetres, and the modulus (MPa) were measured. The specimens were sliced from the nanofibrous mats to a 1.5 × 3 cm dimention pieces and a thickness of between 0.01 and 0.03 mm, which was measured using a digital micrometer. The JQ03B micro tensile testing machine was used to conduct tensile tests (Powereach, Shanghai, made in China).

Swelling test

In PBS, the swelling ability of the crosslinked PVP scaffold was compared to that of the crosslinked Mh treated PVP scaffold at various concentration ratios (15%, 20%, 25%). Weighing the dried ENS (3 cm x 2 cm) and incubating them for 48 h at 37 °C (to simulate normal body temperature) in PBS, followed by two washes with deionised water. The mat's surface water was filtered out using filter paper and the mat was weighed again (W2). The swelling percentage was calculated using the following equation:

$$\text{Swelling}\ (\%)=\frac{W2-W1}{W1}\times 100$$

In vivo studies of wound healing potentials

Evaluation of wound healing potential (animal study)

16 male Swiss albino mice weighing between 180 and 220 g were randomly divided into two groups (test and control) including eight mice each. After administering pentobarbital (45 mg/mL), the dorsal region of the mice was completely depilated with Na2S (8.0%, w/v), and full-thickness circular wounds (1 cm in diameter) were made on the upper back of each mouse using sharp scissors and a scalpel. The scientific ethics committee at Beni-Suef University approved all animal procedures (reference number: 2020-131428). Prior to treatment, the nanofibrous mats were sterilized by electron-beam irradiation using a linear accelerator at a total dose of 100 cGy. The wounds were dressed with conventional wound dressing (G2- test group) and ENS Mh15 percent @ PVP (ENS Mh15 percent PVP) (G1-control group). Each fiber mat in both groups was coated with antiseptic gauze, and the gauze edge was sutured around the incision site. The wound site was inspected following therapy. 1, 2, 4, 6, 8, 10, and 12 days. The wounds of mice were photographed, and the area of the wound that had not healed was assessed using Photoshop. For macroscopical analyses of the wound healing process, the pattern of hair growth, the skin's appearance, and the production of scars were documented.

Histological analysis

Bancroft and Stevens' approaches are followed for histology preparations (Stevens et al. 2004; Bancroft and Gamble 2008) Skin tissue slices were fixed in 10% neutral buffered formalin (NBF), dried in graduated doses of ethanol, cleaned in xylene, and embedded in paraffin for further study. The general tissue structure was analyzed using hematoxylin and eosin stain after the paraffin blocks were sectioned with a microtome at a thickness of (4–6 m).

Cell viability assay

The proliferation and viability of the NIH/3T3 cell line murine fibroblast derived from a mouse NIH/Swiss embryo, Merck, was assessed to evaluate the cell response to PVP, Mh15%@PVP, Mh20%@PVP, Mh25%@PVP, and CT-TiONTs/PVP-15%Mh scaffolds, as well as in the control group (medium

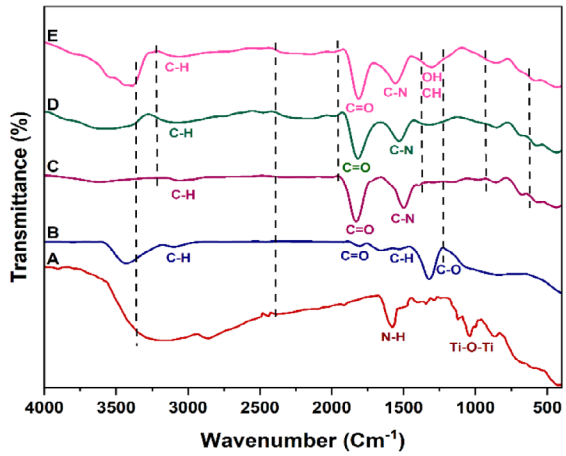

Fig. 2 FTIR depicted a comparison of the spectra of chitosan coated titanate (**A**), pure manuka honey (MH) (**B**), PVP (**C**) and composites of honey treated PVP (**D**) and chitosan titanate loaded Mh@PVP (**E**)

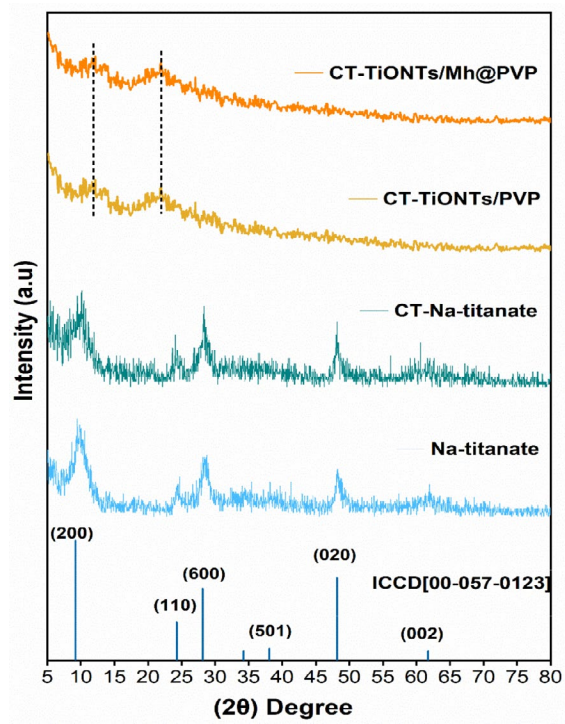

Fig. 3 XRD pattern for the fabricated materials

devoid of scaffolds). MTT dissolved in water (Sigma, US) is converted by enzymes 13 located inside the mitochondria of living cells into the insoluble purple formazan salt. In 96-well plates, fibroblasts were seeded at a density of one million cells per well onto scaffolds. After another four hrs at 37 °C in a humidified environment with 5% CO2, each well was treated with a final concentration of 2.5 mg/mL MTT. For absorbance measurements, dimethyl sulfoxide (DMSO, Sigma) was added to 100 µl of cells and dissolved in water. The cells in the control group were determined to be 100 percent viable. Scaffolds were evaluated using the MTT test after 1 and 2 days.

Statistical analysis

The data are presented as the mean standard deviation. Students' t-test was used for statistical analysis, SPSS version 25 was used to calculate the significance level of the data. Probability value (p) ≤ 0.05 was considered to be statistically significant. ImageJ software V 1.8.0 is utilized for nanofiber diameter analysis.

Results of physicochemical characterization and Discussion

Zeta potential confirms chitosan coverage of titanate nanotubes

Suspensions of TiONts were prepared in 10 M NaCl aqueous solutions. The pH of the suspension was adjusted from 3 to 11 by addition of HCl or NaOH solutions. Indeed, TiONts have a low isoelectric point (IEP) at pH 4 and a negative zeta potential at an acidic pH (> 4), owing to the presence of numerous hydroxyl groups on their surface. As a positively charged polymer, chitosan grafting increases the (potential to approximately + 30 mV. Zeta potential measurements on TiONts and CT-TiONTs demonstrate a significant increase in the nanotubes' (IEP), from pH 3.6 for bare nanotubes to pH 10.2 for CT-TiONts. The increase in IEP indicates that the surface of TiONts has been charged positively due to the presence of amine functionalities. By increasing the zeta potential of the synthesized nanohybrid to more than + 30 mV, chitosan grafting significantly improves its colloidal stability (Between pH 3 and 5). In this range, pure chitosan has a potential of approximately + 40 mV. CT-TiONts-nanohybrids have the same potential for evolution as pure chitosan, but at a lower rate due to the presence of TiONts' hydroxyl groups. This result demonstrates that chitosan grafting of TiONts, as investigated by F Sallem et al., exhibits a similar pattern of behaviour (Sallem et al. 2017).

FT-IR and XRD analysis

Figure 2 illustrates FTIR. The spectra of pure Mh, PVP, and Mh@PVP composites, as well as chitosan-coated titanate, were compared to those of CT-TiONTs/Mh@PVP. The spectra of pure Mh dopant contained distinctive peaks near 1226 cm^{-1}, 1459 cm^{-1}, 1729 cm^{-1}, and 3178 cm^{-1}, which are attributed to C–O, C–H, and C=O stretching and bending vibrations characteristic of Mh and its simple sugars and are consistent with previous studies(Ghalei et al. 2021). Figure 2A The peaks at 1583, 1812, and 3074 cm^{-1} were attributed to NH bending, CO–NHR, and CH respectively that are characteristic to chitosan(Khan and Dhayal 2008). The wide peak at 848 cm^{-1} corresponds to the Ti–O–Ti frequency range (Payan et al. 2018). In Fig. 2A the 672 cm^{-1} is the crystalline sensitivity band of OH(Çay et al. 2014). It was stripped away from the composite as a result of chitosan's hydrogen bonding with acetic acid and PVA, as well as the action of honey's saccharide wagging band, indicating that the chitosan has become less crystalline, as confirmed by XRD analysis. Given that hydrogen bonding reduces the frequency of stretching vibrations, this implies that hydrogen bonds are formed between chitosan and TiONa via NH_2(D'Avila Carvalho Erbetta et al. 2012). Figure 2E a 1307 cm^{-1} overtone peak recognized the saccharide function groups of honey (glucose and fructose), PVP and chitosan (Homayoni et al. 2009). Furthermore, the 1504 and 1564 cm^{-1} peaks were generated by the coupling of OH in-plane and CH wagging vibrations. Bands at 1033 and 1123 cm^{-1} are caused by hydrogen bonding between the hydroxyl and amino groups, respectively (Khan and Dhayal 2008). PVP's 1828 cm^{-1} band shifted to 1807 cm^{-1} as a result of O–C–NH_2, confirming the presence of titanates in the composite. The 1315 cm^{-1} peak corresponds to the CH bond in PVP; the peak's intensity was decreased in the composites (Zidan et al. 2019).

Other distinctive peaks, such as 1569, 1814, and 1957 cm^{-1}, also indicate the presence of PVP in the vicinity of manuka honey and chitosan. Between 3382 and 3400 cm^{-1}, a broad band was observed due to the stretching vibration of the OH group, which revealed a distinct peak for both chitosan and PVP. In the composites, some peaks changed to a lower frequency, while others vanished, and new ones developed. The two distinct bands of Mh at 1314 and 3426 cm^{-1} in Fig. 2C (Mh@PVP composite) vanished in Fig. 2D due to the successful incorporation of Mh in PVP and the low honey-to-PVP ratio. CT-TiONTs/Mh@PVP At 1301 and 3382 cm^{-1}, two new distinct bands appeared (Fig. 2E). The broad band between 3267 and 3365 cm^{-1} was attributed to the stretching vibration of the OH group, which revealed a characteristic peak for both chitosan and PVP. Due to the lack of a sharp peak, chitosan's hydroxyl groups in positions C2 and C6 are connected via intramolecular and intermolecular hydrogen bonds(D'Avila Carvalho Erbetta et al. 2012). As a result of the FTIR analysis, it was determined that the composite scaffold contained Manuka honey, PVP, chitosan, and sodium titanate. Chitosan-titanate can be homogeneously incorporated into Mh@PVP composites through the action of hydrogen bonding forces between the OH or NH_2 of chitosan and the OH or NH_2 of PVP. This indicates that the chitosan, as determined by XRD measurements, has become less crystalline. The electrostatic interactions between the amines in chitosan and the hydroxyl groups in nanotubes drive the chitosan grafting process. The electrostatic approach has the advantage of being straightforward to apply and well-suited for drug delivery systems due to its low binding energy, which can be rapidly dissolved and capable of releasing the therapeutic molecule into the targeted tissue(Sallem et al. 2017).

Patterns of X-ray diffraction (XRD) were used by Cu-Kα radiation (wavelength λ = 1.54060 Å) at an accelerating voltage of 40 kV, current of 30 mA, the scan range of 5°–80°, and the scan step of 0:05º, divergence Slit (fixed). Figure 3 illustrates the XRD-determined diffraction patterns of CT-TiONTs, pure PVP, and Mh@PVP nanofibers incorporating CT-TiONTs. The incorporation of CT-TiONTs nanotubes into either pure PVP or Mh@PVP nanofibers resulted in a decrease in the intensity of the titanate and chitosan crystallinity peaks, indicating a high prevalence of poorly crystalline phase within the sample and lending support to the poor crystallinity nature of polymer PVP electrolyte (at 12 &22 degrees, two broad, low-intensity peaks were observed). PVP increases ionic diffusivity, which improves conductivity. When PVP is electrospun into nanofibers, its amorphous microstructure is further harmed. The low percentage of CT-TiONTs nanotubes in the parent PVP or Mh@PVP solution before electrospinning and the difficulty to perform annealing due to the heat-sensitive nature of manuka honey are additional variables influencing this amorphous XRD behaviour. Our findings match the previously published XRD diffraction patterns of pure polyvinyl pyrrolidine, manuka honey, and chitosan-coated titanate by Kuchi et al. and Fuentes et al. (Kuchi et al. 2018; Fuentes et al. 2020). The Mh treatment of PVP and the addition of chitosan titanate were unable to enhance the poor crystallinity of PVP, the primary component of the CT-TiONTs/Mh@PVP composite electrospun nanofibers, as compared to the cast film.

Surface morphological shape, SEM analysis

The morphology of ENSs was analysed using SEM images. The electrospun nanofiber diameters were estimated by measuring fiber diameters in SEM images using ImageJ 1.53 K (National Institute of Health, Bethesda, MD, USA) software and then averaging them. For samples A, B, C and E, the mean fiber diameter was determined using an average of 80 fibers; however, for sample D, the average mean was computed using only the 35 fibers visible in the image due to the increasing diameter of the fibers. As seen in Fig. 4C, The Mh15%@PVP scaffold enabled the most homogeneous distribution of nanofiber diameters, with the majority of nanofibers having diameters between 300 and 450 nm, with average of 37 nm. Whereas Mh20%@PVP and Mh25%@PVP scaffolds resulted in nonhomogeneous, a wide range of.fiber diameter distribution (Fig. 4A, B, and D). In Fig. 4D, the nanofiber diameter grew from nanoscale to microscale after crosslinking at 50 °C, which may be attributed to the deterioration of mauka honey caused by exposure to heat. The average diameter of Mh@PVP nanofibers increased (37 to 368 nm) as the honey concentration was increased from 15 to 25%, which is consistent with the study of Sarhan et al. (Sarhan et al. 2016).

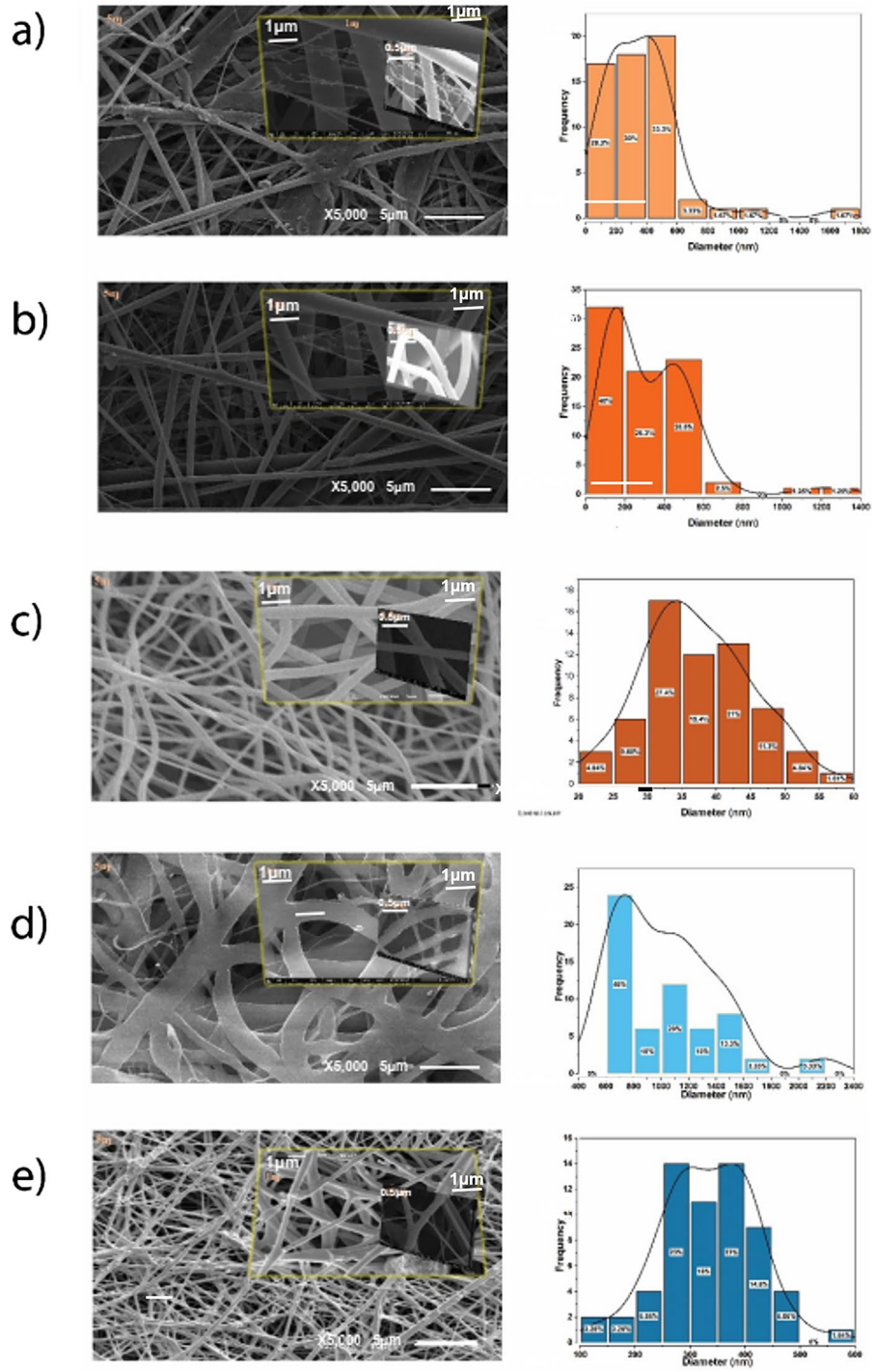

Fig. 4 SEM analysis, **a:** Mh25%@PVP scaffold, **b:** Mh20%@PVP scaffold, **c:** Mh15%@PVP scaffold, **d:** Mh15%@PVP scaffold crosslinked at 50 °C, **e:** Mh15%@PVP scaffold crosslinked at 30 °C. SEM images under 5 k magnification for [Sample: mean fiber diameter ± standard deviation (SD) in (µM)]: [a: 0.368 ±0.261]; [b: 0.257 ± 0.224]; [c: 0.37 ± 0.07; [d: 1.038 ± 0.375], [e: 0.397 ± 0.47]

It is claimed that increasing the amount of Mh in a solution increases the number of ions in it, decreasing the solution's viscosity and increasing its conductivity. As shown in Fig. 4, increasing the honey content increased the diameter of the nanofibers; additionally, the scaffold has a rough surface with irregular fiber orientation (Fig. 4a, b and c). The highest honey to polymer ratio cause beads and heterogenous

Table 2 Mechanical properties Summary

Property		Electrospun Naofiberous Scaffold				
		PVP	Mh 15% @PVP	Mh 20% @PVP	Mh 25% @PVP	CT-TiONTs/ Mh 15% @ PVP
Viscosity (Pa.s)		178	131	108	97	147
Electrical conductivity (µs)		314	572	928	1360	583
Average tensile strength (Newton)	Wet	2.41	2.06	3.24	4.65	2.17
	Dry	3.37	3.85	5.48	6.1	3.79
Water contact angle (Degree)		42.12 ± 1.62°	38.87 ± 1.09°	32 ± 2.37°	24.16 ± 1.4°	36.87 ± 0.43°

distribution of fiber diameter reaching the micro size. Appropriate honey to polymer ratios were seen in the non-crosslinked and crosslinked Mh15%@PVP samples c and e, narrower, homogenous and smoother nanofibers compared to sample a, b and d which have a rough surface and irregular fiber orientations (Fig. 4 and Table 1). Maleki et al. (2013) study's demonstrated similar results. Appropriate amounts of honey help to overcome the challenges associated with high polymer concentrations by keeping the fiber diameter in the nanoscale range.

Electrical conductivity changes by incorporation of Mh into the PVP polymer

The electric conductivity of the solutions was measured using

Prior to electrospinning, the conductivity and viscosity of aged polyvinyl PVP (15%) solutions with increasing honey concentrations (15, 20, and 25%) were measured (Table 2), using a Radelkis OK-102/1 conductivity meter and a HAAKE Roto Visco rheometer at 25° C. The increased percentage of Mh in the 15% PVP solutions caused a considerable change in the conductivity of the solutions, which increased from 572 uS with 15% Mh@PVP to 928 uS with 20% Mh@PVP and 1360 uS with 25% Mh@PVP, respectively. Due to the fact that conductivity is related to the amount of ions in a solution, which rises as honey content rises, raising the polymer concentration may permit the integration of a greater proportion of honey. The electrical conductivity measurements of samples revealed that the addition of honey to PVP solution led to a rise in the electrical conductivity. The investigation conducted by FC Allolu et al. yielded comparable results (Çallıoğlu et al. 2019).

Mechanical properties

The list of PVP, Mh15%@PVP, Mh20%@PVP, Mh25%@PVP and CT-TiONTs/Mh15%@PVP samples mechanical characteristics, including their conductivities and viscosities, tensile strengths and water angle, is shown in Table 2.

Tensile Properties

Tensile stress tests were conducted on crosslinked PVP mats with and without varying percentages of Mh (15%, 20%, and 25%) and the results are described in Table 2. Mechanical properties of the scaffolds were significantly improved when dry scaffolds were used, particularly at 20% and 25% Mh concentrations. By role, moist scaffolds demonstrated poorer strength than dry scaffolds. Honey addition resulted in an improved in the mechanical strength of the Mh@PVP scaffolds, similar findings were published by the study of S. Ghalie et al. on polylactic acid (PLA) nanofibers mat (Ghalei et al. 2021). The inclusion of honey can result in the formation of additional interpolymer linkages, resulting in a noticeable increase in the mechanical strength of Mh@PVP due to the increased physical cross-linking density.

Wettability

A properly fitted dressing should be able to absorb wound exudates while also retaining moisture at the wound site. These parameters are influenced by the wettability and hydrophilicity of the dressing's

surface. Wettability of manufactured dressings was determined using the water contact angle method. The water contact angles of crosslinked pure PVP and Mh15%@PVP, Mh20%@PVP and Mh25%@PVP nanofibers were 42.12 ± 1.62°, 38.87 ± 1.09°, 32 ± 2.37°, and 24 ± 1.4°, respectively, Table 2. These results indicate that the addition of increasing amounts of manuka honey decreases the water contact angle, proving the hydrophilicity of the Mh@PVP-fabricated scaffolds, making them appropriate for absorbing exudates and maintaining the moisture content of the wound dressing. A higher honey content improves the surface wettability of polyurethane mats while reducing the hydrophobicity of poly(1,4-cyclohexane dimethylene isosorbide trephthalate) scaffolds (Khan et al. 2017; Parin et al. 2021).

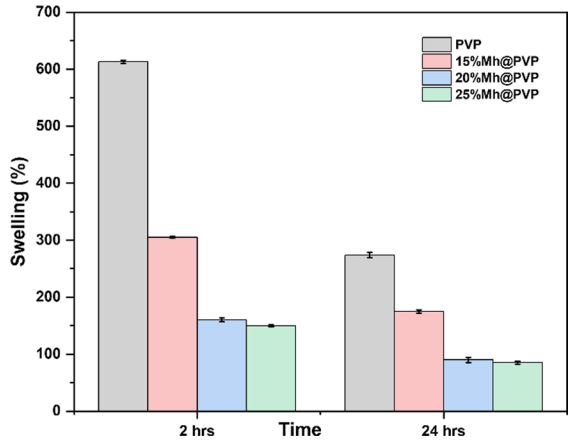

Fig. 5 PVP (control) and Mh 15%@PVP, Mh 20%@PVP, and Mh25%@PVP (test) swelling ratio profiles after 2 and 24 h

Permeability of water vapor (PWV)

PWV is an important parameter for characterization of wound dressing textile (Türkoğlu et al. 2021). The vapor exchange rate of the dressing is a vital feature that determines its efficacy (Nuutila and Eriksson 2021). A high PWV value dehydrates the wound and promotes scar formation, whereas a low PWV value retards the wound healing process due to exudate deposition. As a result, a suitable dressing should have an optimal PWV value. The results indicated that the PWV value for PVP scaffolds was 18.57 ± 1.34 mg/cm^2/hr, whereas honey reduced this value to 11.73 ± 1.04 (60%) mg/cm^2/hr in CT-TiONTs/Mh15%@PVP. These findings indicate that the manufactured CT-TiONTs/Mh15%@PVP can effectively absorb wound exudates and thereby aid in the wound healing process.

Swelling ratio

Figure 5 illustrates the swelling profile of the PVP scaffolds produced without (control) and with various concentrations of honey (15%, 20% and 25%). Once soaked in PBS, it is thought that all PVP scaffolds commence the absorption process; initial uptake of water after 2 h due to the presence of honey increases scaffold degradation rates; however, scaffold degradation rates were reduced dramatically after 24 h. Our findings support those of Ghorbani et al. that swelling ability is decreased by increasing the honey concentration within the PVP scaffold (Ghorbani et al. 2021). Due to honey's high-water solubility, the degree of degradation of NFs increases, resulting in the loss of the nanofibers scaffold's compacted porous structure and its capability of retaining water and by its role it diminishes it's swelling ability. Mh15% @PVP scaffold demonstrates an appropriate swelling ratio when compared to scaffolds with larger concentrations of included honey (Mh20% @PVP and Mh25% @PVP) that support the needed function of a wound dressing by facilitating the absorption of wound exudate and keep the media hydrate. Based on the hygroscopic nature of honey the swelling capacity of the scaffold dependent on the composition and ratio of blends.

Invitro Mh release (methylglyoxal (MGO) Assay)

The Mh release from the soaked scaffolds was determined as an indication of the methylglyoxal release. Each one of the crosslinked Mh15%@PVP, Mh20%@PVP, Mh25%@PVP scaffolds were immersed in 1 litter of sterile (PBS) phosphate buffer solution (900 mL, 120 rpm, 37 °C). At 1 h and then every 24 h for 7 days, the PBS was retained and replaced, the cumulative percentage was calculated using UV spectroscopy.

The methylglyoxal release was monitored over a 7-day period (Fig. 6), and it exhibited two distinct kinetic releasing patterns: burst followed by continuous release. For the first 24 h, Mh15%@PVP scaffolds released approximately 40% of methylglyoxal;

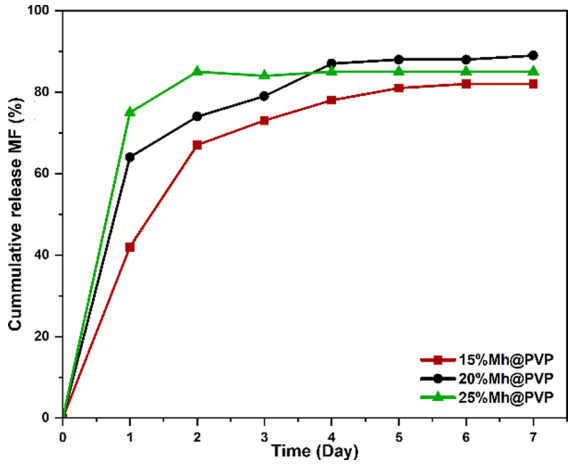

Fig. 6 Methylglyoxal assay for detection of Mh release in the biologically simulated PBS media

whereas, Mh20%@PVP and Mh25%@PVP scaffolds released between 60 and 70% of methylglyoxal, respectively. After two days, the release steadily decreased from Mh15%@PVP and Mh20%@PVP to PVP-25%Mh, which occurred on days five and seven in Mh15%@PVP and Mh20%@PVP, respectively, and the scaffolds were substantially degraded, in accordance with Hixon et al. (Hixon et al. 2017). The methylglyoxal assay in phosphate buffered saline reveals two distinct patterns of methylglyoxal release from manuka honey, including burst release followed by continuous release for up to seven days, which is encouraging for promoting the healing process. This demonstrates the sustained release of methylglyoxal as Mh@PVP scaffolds disintegrate, particularly during the initial days, thereby assisting the body's natural fibrin mat synthesis and thereby accelerating the healing process. The degradation process is accelerated by increasing the proportion of honey in the scaffold. Due to the high-water solubility of non-crosslinked Mh@PVP scaffolds, we were unable to conduct this experiment.

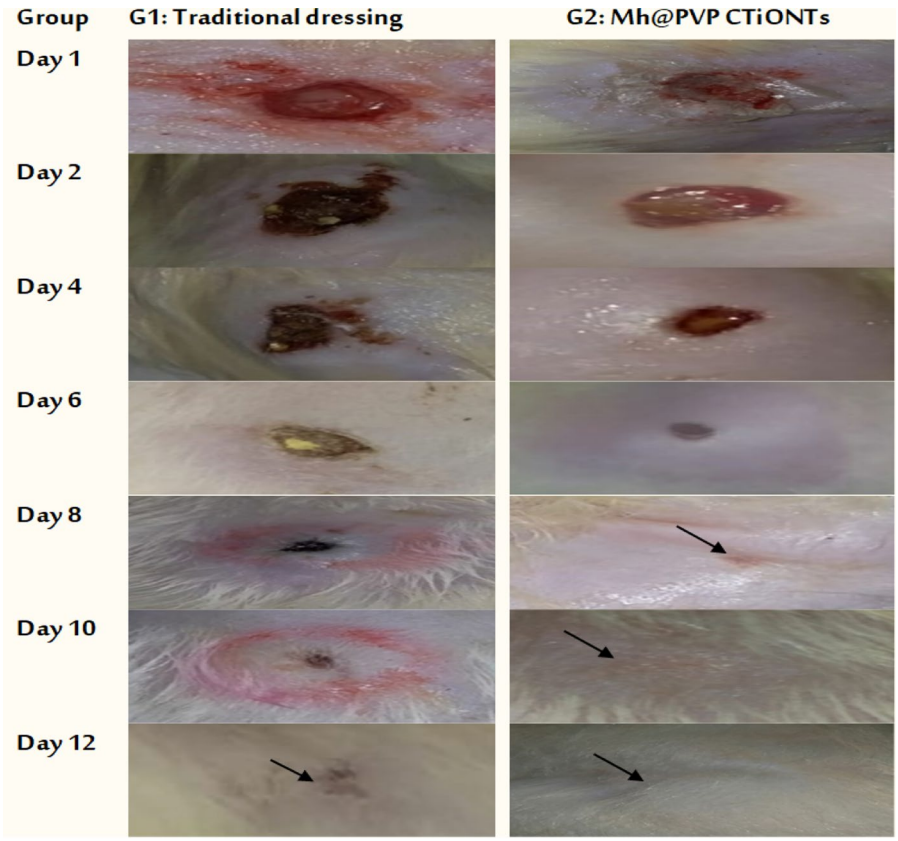

Fig. 7 Macroscopic appearance of wound healing on male Swiss albino mice of at different times (Days 1, 2, 4, 6, 8, 10, 12)

Table 3 Wound size reduction (%) in comparison to day 1 for control (G1) and test (G2) groups, H for hair, S for scar. The significance of variations in average values between test and controls has been determined and expressed as mean ± SD

Days	Wound healing (%) ± SD G1(traditional dressing)	H	S	Wound healing (%) ± SD G2 advanced dressing	H	S
1	0	×	×	0	×	×
2	0	×	×	13 ± 6.5	×	×
4	24 ± 9.1	×	×	76 ± 8.3	×	×
6	36 ± 3.7	×	×	100 ± 9.5	×	×
8	79 ± 8.9	×	×	100	✓	×
10	93 ± 4.5	✓	✓	100	✓	×
12	95 ± 2.6	✓	✓	100	✓	×

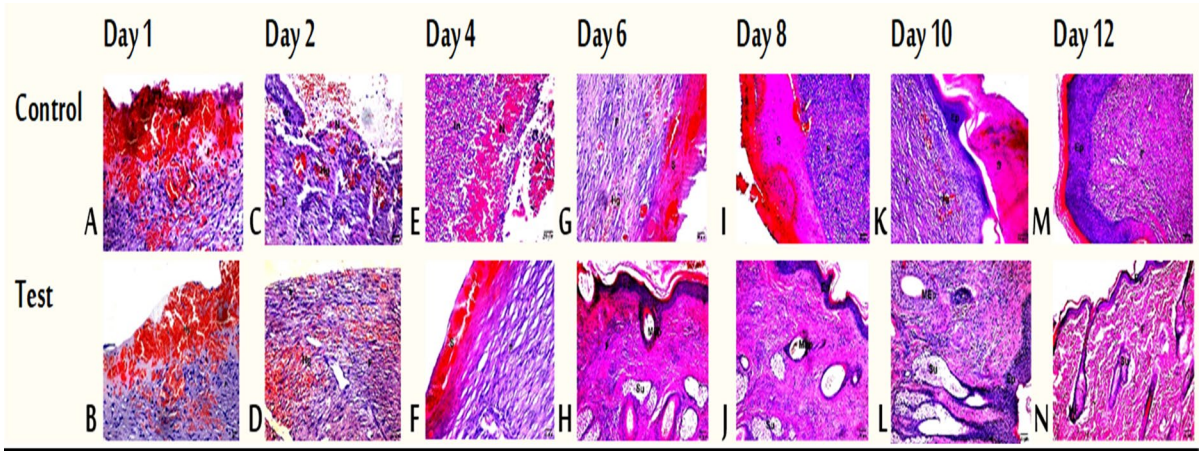

Fig. 8 Histopathological evaluation of skin sections (Days 1 to 12)

In vivo studies of wound healing potentials

Assessment of Wound healing capabilities

On the dorsal back of mice, an excisional 1 cm diameter circular wound was covered with the ENS Mh15%@PVP mats (G2-control group) and a commercially available traditional wound dressing (G1-test group). On days 1, 2, 4, 6, 8, 10 and 12, (Fig. 7). A significant difference in the extent and the quality (hair growth with no scar) of wound healing amongst the advanced dressing (Mh@PVP) as compared to the traditional dressing (control) dressings was observed. On day four, it was noticed that the test group's wound edges had begun to epithelialize, resulting in a reduction in wound size. However, on the day 6, the appearance and differences between both groups was clear supporting the efficacy of Mh@PVP dressing. Day 8, it has been observed that the test group showed accelerated and high-quality healing (wound closure) with hair growth and scar free healing compared to control (79% ± 8.9). Additionally, the immunomodulatory impact of Mh accelerates the healing process and increases fibroblast proliferation, resulting in higher collagen synthesis and decreased scar formation (Muktar et al. 2018). Evaluations of wounds indicated that dressings immobilized with manuka honey were extremely effective for preventing scarring at the wound site. Manuka honey is claimed to provide therapeutic benefits over other honeys and to aid in the healing process by providing glycogen to epithelial cells. Additionally, the antioxidant phytochemical components contribute significantly to the reduction of inflammation (Molan and Rhodes 2015). Table 3 and Fig. 7 provide a comparison of the percentage of wound size reduction and the wound's observed appearance (quality of healing, hair and scar).

$$\text{Wound size (\%)} = \frac{wound\ size\ on\ day\ 1 - wound\ size\ on\ day\ (x)}{wound\ size\ on\ day\ 1} \times 100$$

Assessment of the histological outcomes

If we look microscopically at Fig. 8, we were able to observe the various stages of wound healing in the skin of the control and tested groups using photomicrographs from day 1 to day 12. At DAY 1, haemorrhage, mononuclear inflammatory cell infiltration, and the formation of fibrous connective tissue were observed in both the control and test groups (Section A and B). Section C (control group) exhibits hemorrhage and necrotic tissue at the wound's periphery, as well as mononuclear inflammatory cell infiltration and the formation of fibrous connective tissue, whereas Section D (test group) exhibits hemorrhage and fibrous connective tissue formation with a reduced number of inflammatory cells. On DAY 4, Section E (control group) exhibited necrotic tissue surrounded by a dense population of inflammatory cells, whereas Section F (test group) exhibited the formation of fibrous connective tissue as well as edema and scab. On DAY 6, despite the presence of an epidermal layer, migrating epidermal cells, and a suspicious gland in Section H (test group), Section G (control group) demonstrated the formation of fibrous connective tissue with hemorrhage and a scab (H&E Staining). On DAY 8, Section I (control group) demonstrates the development of fibrous connective tissue that is covered by a thick scab. The formation of increasing epidermal layers, migrating epidermal cells, and suspicious glands is demonstrated in Section J (test group). On DAY 10, Section K (control group) had fibrous connective tissue with hemorrhage and several layers of epidermis covered in a thick scab, whereas Section L (test group) had suspicious glands, some of which attempted to open into the epidermis, as well as migrating epidermal cells. On day 12, Section M (control group) displayed conspicuous fibrous connective tissue covered by epidermis, while Section N (test group) displayed normal histological appearance of skin in its epidermis, fibrous tissue, suspicious glands, and hair follicle. Histological analysis revealed that when compared to a conventional dressing, the optimally fabricated Mh15%@PVP nanofibrous dressings significantly reduced necrosis, with the greatest reduction occurring after day 6. In comparison to the negative control, the Mh15%@PVP dressings induced early epithelization with the formation of mature granulation tissue and a thicker observed epidermis. Additionally, suspicious glands and hair follicles indicate a rapid and high-quality wound healing.

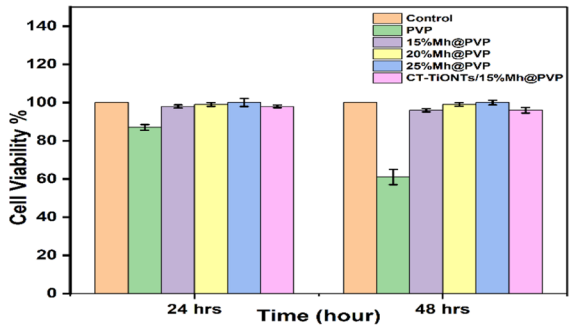

Fig. 9 The MTT assay for five developed nanofibrous mats: PVP, Mh@PVP containing increasing amounts of Mh (15%, 20%, 25%), and traditional dressing as a control. The mean standard deviation is given (Student's t-test, *p-value 0.05 culture times 24 h & 24 h)

Cell viability assay

The wound healing process is known by its complexity and interaction of different cell types with matrix components that act together to re-establish the 3D structure and the functions of the damaged tissue. Herein, The proliferation and viability of the NIH/3T3 fibroblast cell line was assessed to evaluate the cell response to PVP, Mh15%@PVP, Mh20%@PVP, Mh25%@PVP, and CT-TiONTs/PVP-15%Mh scaffolds, as well as in the control group (medium devoid of scaffolds). Figure 8 demonstrates that there were no significantly significant differences between the control and test groups ($p > 0.01$), with the exception of the PVP scaffold (after 24 and 48 h), which may be attributed to manuka honey's capacity to promote oxygen and nutrient transport to cells while decreasing viable cell count ($p > 0.01$). Nonetheless, cell viability analysis revealed that more than 90% of viable cells were present in all scaffolds. Additionally, when compared to other scaffolds studied, PVP-25% Mh was associated with a higher percentage of cell

viability on days 1 and 2. One possible explanation is that the scaffold's stiffness-elasticity balance is improved as a result of the addition of more manuka honey, a slower degradation rate, acceptable biomechanical properties, and an appropriate ratio of hydrophilic to hydrophobic groups (Fig. 9).

Conclusion

This study demonstrated the fabrication of an advanced electrospun wound dressing from a PVP and Mh composite that was loaded with chitosan grafted titanate as a nanocarrier. Using a highly concentrated PVP solution allows for higher manuka honey incorporation while reducing the flattening or beading morphology caused by high honey concentration. SEM images and mechanical tests confirmed that PVP with 15% Mh gave the best scaffolds with improved mechanical properties. Due to the heat sensitivity of manuka honey, the processes of fabrication, crosslinking, and storage of the PVP-Mh electrospun mat require specific temperatures. Applying manuka honey topically helps prevent wound infections, accelerates wound healing, and slows the spread of necrotizing fasciitis. Our preclinical and histological studies demonstrated that PVP-Mh dressings improve the quality of wound healing and skin regeneration, resulting in scarless regrowth of hair. By incorporating manuka honey into PVP, electrospun nanofibrous scaffolds gain increased wettability and permeability, allowing them to absorb exudates and retain moisture in the wound bed. Due to the honey's low toxicity, our cell viability studies show that the more honey you use, the more benefits you get. This promising combination can be used to target drug delivery, improving and speeding up the healing process in patients with chronic wounds like diabetic foot and bedsores.

Acknowledgements Technical assistance is gratefully acknowledged for the central lab personnel of the Faculty of Postgraduate Studies for Advanced Sciences, Beni-Suef University, Egypt.

Author contributions LM, AG and SI designed of the experiments. LM, AH, and AG conducted the tests. LM and AH performed data analysis. LM and AG wrote the original manuscript. The final manuscript was revised and approved by all authors.

Funding Open access funding provided by The Science, Technology & Innovation Funding Authority (STDF) in cooperation with The Egyptian Knowledge Bank (EKB). This research was not supported by any public, private, or non-profit funding organizations.

Data and materials availability This publication contains all of the information analyzed during this investigation. Additional raw data required to replicate these findings are available from the corresponding author upon reasonable request.

Declarations

Conflict of interest The authors report that they are unaware of any competing financial interests or personal ties that may have influenced the work presented in this study.

Ethics approval Not applicable.

Consent for publication Not applicable.

References

Adams CJ, Manley-Harris M, Molan PC (2009) The origin of methylglyoxal in New Zealand Manuka (Leptospermum scoparium) honey. Carbohydr Res 344:1050–1053. https://doi.org/10.1016/j.carres.2009.03.020

Ahmed A, Xu L (2020) Numerical analysis of the electrospinning process for fabrication of composite fibers. Therm Sci 24:2377–2383. https://doi.org/10.2298/TSCI200437A

Alipour R, Khorshidi A, Shojaei AF et al (2019) Skin wound healing acceleration by Ag nanoparticles embedded in PVA/PVP/Pectin/Mafenide acetate composite nanofibers. Polym Test 79:106022

Atrott J, Haberlau S, Henle T (2012) Studies on the formation of methylglyoxal from dihydroxyacetone in Manuka (Leptospermum scoparium) honey. Carbohydr Res 361:7–11. https://doi.org/10.1016/j.carres.2012.07.025

Augustine R, Rehman SRU, Ahmed R et al (2020) Electrospun chitosan membranes containing bioactive and therapeutic agents for enhanced wound healing. Int J Biol Macromol

156:153–170. https://doi.org/10.1016/j.ijbiomac.2020.03.207

Aytimur A, Uslu I (2014) Promising materials for wound dressing: PVA/PAA/PVP electrospun nanofibers. Polym Plast Technol Eng 53:655–660. https://doi.org/10.1080/03602559.2013.874031

Baati T, Njim L, Jaafoura S et al (2021) Assessment of pharmacokinetics, toxicity, and biodistribution of a high dose of titanate nanotubes following intravenous injection in mice: a promising nanosystem of medical interest. ACS Omega 6:21872–21883. https://doi.org/10.1021/acsomega.1c01733

Badet C, Quero F (2011) The in vitro effect of manuka honeys on growth and adherence of oral bacteria. Anaerobe 17:19–22. https://doi.org/10.1016/j.anaerobe.2010.12.007

Bancroft JD, Gamble M (2008) Theory and practice of histological techniques. Elsevier health sciences, Amsterdam

Blair SE, Cokcetin NN, Harry EJ, Carter DA (2009) The unusual antibacterial activity of medical-grade Leptospermum honey: antibacterial spectrum, resistance and transcriptome analysis. Eur J Clin Microbiol Infect Dis 28:1199–1208. https://doi.org/10.1007/s10096-009-0763-z

Bogdanov S (2015) Honey as nutrient and functional food: a review. Bee Prod Sci 1100:1–47

Boudon J, Sallem F, Loiseau A et al (2021) Development of novel versatile theranostic platforms based on titanate nanotubes: towards safe nanocarriers for biomedical applications. In: Abadie M, Pinteala M, Rotaru A (eds) New trends in macromolecular and supramolecular chemistry for biological applications. Springer, Berlin, pp 151–178. https://doi.org/10.1007/978-3-030-57456-7_8

Çallıoğlu FC, Güler HK, Çetin ES (2019) Emulsion electrospinning of bicomponent poly (vinyl pyrrolidone)/gelatin nanofibers with thyme essential oil. Mater Res Express 6:125013

Cavallaro G, Micciulla S, Chiappisi L, Lazzara G (2021) Chitosan-based smart hybrid materials: a physico-chemical perspective. J Mater Chem B 9:594–611. https://doi.org/10.1039/D0TB01865A

Çay A, Miraftab M, Kumbasar EPA (2014) Characterization and swelling performance of physically stabilized electrospun poly (vinyl alcohol)/chitosan nanofibres. Eur Polym J 61:253–262. https://doi.org/10.1016/j.eurpolymj.2014.10.017

Contardi M, Kossyvaki D, Picone P et al (2021) Electrospun polyvinylpyrrolidone (PVP) hydrogels containing hydroxycinnamic acid derivatives as potential wound dressings. Chem Eng J 409:128144. https://doi.org/10.1016/j.cej.2020.128144

Cooper RA, Halas E, Molan PC (2002) The efficacy of honey in inhibiting strains of Pseudomonas aeruginosa from infected burns. J Burn Care Rehabil 23:366–370. https://doi.org/10.1097/00004630-200211000-00002

Cooper RA, Lindsay E, Molan PC (2011) Testing the susceptibility to manuka honey of streptococci isolated from wound swabs. J Apiprod Apimed Sci 3:117–122. https://doi.org/10.3896/IBRA.4.03.3.02

D'Avila Carvalho Erbetta C, Alves RJ, Resende JM et al (2012) Synthesis and Characterization of Synthesis and Characterization of poly (D, L-lactide-co-glycolide) copolymer. J Biomater Nanobiotechnol 3:208–225. https://doi.org/10.4236/jbnb.2012.32027

Deng J, Liu R, Lu Q et al (2018) Biochemical properties, antibacterial and cellular antioxidant activities of buckwheat honey in comparison to manuka honey. Food Chem 252:243–249. https://doi.org/10.1016/j.foodchem.2018.01.115

El Nahrawy AM, Hemdan BA, Abou Hammad AB (2021) Morphological, impedance and terahertz properties of zinc titanate/Fe3+ nanocrystalline for suppression of Pseudomonas aeruginosa biofilm. Nano-Struct Nano-Object 26:100715. https://doi.org/10.1016/j.nanoso.2021.100715

El-Senduny FF, Hegazi NM, Abd Elghani GE, Farag MA (2021) Manuka honey, a unique mono-floral honey. A comprehensive review of its bioactives, metabolism, action mechanisms, and therapeutic merits. Food Biosci 42:101038. https://doi.org/10.1016/j.foodchem.2018.01.115

Farghali AA, Zaki AH, Khedr MH (2016) Control of selectivity in heterogeneous photocatalysis by tuning TiO2 morphology for water treatment applications. Nanomater Nanotechnol 6:12. https://doi.org/10.5772/62296

Fuentes S, León J, Vega JL, Zenteno S (2020) Chitosan coating of BaTiO3@ ZnO: Yb heterostructures: synthesis and properties. J Sol-Gel Sci Technol 95:465–473. https://doi.org/10.1007/s10971-020-05329-5

Georgescu M, Chifiriuc C, M, Marutescu L, et al (2017) Bioactive wound dressings for the management of chronic wounds. Curr Org Chem 21:53–63. https://doi.org/10.2174/1385272820666160510171040

Gethin G, Cowman S (2005) Case series of use of Manuka honey in leg ulceration. Int Wound J 2:10–15. https://doi.org/10.1111/j.1742-4801.2005.00078.x

Gethin G, Cowman S (2008) Bacteriological changes in sloughy venous leg ulcers treated with manuka honey or hydrogel: an RCT. J Wound Care 17:241–247. https://doi.org/10.12968/jowc.2008.17.6.29583

Gethin GT, Cowman S, Conroy RM (2008) The impact of Manuka honey dressings on the surface pH of chronic wounds. Int Wound J 5:185–194. https://doi.org/10.1111/j.1742-481X.2007.00424.x

Ghalei S, Li J, Douglass M et al (2021) Synergistic approach to develop antibacterial electrospun scaffolds using honey and S-nitroso-N-acetyl penicillamine. ACS Biomater Sci Eng 7:517–526. https://doi.org/10.1021/acsbiomaterials.0c01411

Ghorbani M, Ramezani S, Rashidi M-R (2021) Fabrication of honey-loaded ethylcellulose/gum tragacanth nanofibers as an effective antibacterial wound dressing. Colloids Surfaces a Physicochem Eng Asp 621:126615. https://doi.org/10.1016/j.colsurfa.2021.126615

Głąb M, Kudłacik-Kramarczyk S, Drabczyk A et al (2021) Hydroxyapatite obtained via the wet precipitation method and PVP/PVA matrix as components of polymer-ceramic composites for biomedical applications. Molecules 26:4268. https://doi.org/10.3390/molecules26144268

Habiba U, Islam MS, Siddique TA et al (2016) Adsorption and photocatalytic degradation of anionic dyes on Chitosan/PVA/Na–Titanate/TiO2 composites synthesized by

solution casting method. Carbohydr Polym 149:317–331. https://doi.org/10.1016/j.carbpol.2016.04.127
Henriques AF, Jenkins RE, Burton NF, Cooper RA (2010) The intracellular effects of manuka honey on Staphylococcus aureus. Eur J Clin Microbiol Infect Dis 29:45–50. https://doi.org/10.1007/s10096-009-0817-2
Henriques AF, Jenkins RE, Burton NF, Cooper RA (2011) The effect of manuka honey on the structure of Pseudomonas aeruginosa. Eur J Clin Microbiol Infect Dis 30:167–171. https://doi.org/10.1007/s10096-010-1065-1
Hixon KR, Lu T, McBride-Gagyi SH et al (2017) A comparison of tissue engineering scaffolds incorporated with Manuka honey of varying UMF. Biomed Res Int. https://doi.org/10.1155/2017/4843065
Homayoni H, Ravandi SAH, Valizadeh M (2009) Electrospinning of chitosan nanofibers: processing optimization. Carbohydr Polym 77:656–661. https://doi.org/10.1016/j.carbpol.2009.02.008
Jeckson TA, Neo YP, Sisinthy SP, Gorain B (2021) Delivery of therapeutics from layer-by-layer electrospun nanofiber matrix for wound healing: an update. J Pharm Sci 110:635–653. https://doi.org/10.1016/j.xphs.2020.10.003
Jose M, Szymańska K, Szymański K et al (2020) Effect of copper salts on the characteristics and antibacterial activity of Cu-modified titanate nanotubes. J Environ Chem Eng 8:104550. https://doi.org/10.1016/j.foodchem.2020.127789
Kato Y, Kishi Y, Okano Y et al (2021) Methylglyoxal binds to amines in honey matrix and 2′-methoxyacetophenone is released in gaseous form into the headspace on the heating of manuka honey. Food Chem 337:127789. https://doi.org/10.1016/j.foodchem.2020.127789
Khan R, Dhayal M (2008) Nanocrystalline bioactive TiO2–chitosan impedimetric immunosensor for ochratoxin-A. Electrochem Commun 10:492–495
Khan MQ, Lee H, Khatri Z et al (2017) Fabrication and characterization of nanofibers of honey/poly (1, 4-cyclohexane dimethylene isosorbide trephthalate) by electrospinning. Mater Sci Eng C 81:247–251. https://doi.org/10.1016/j.msec.2017.08.011
Kuchi C, Harish GS, Reddy PS (2018) Effect of polymer concentration, needle diameter and annealing temperature on TiO2-PVP composite nanofibers synthesized by electrospinning technique. Ceram Int 44:5266–5272. https://doi.org/10.1016/j.ceramint.2017.12.138
Liu X, Xu H, Zhang M, Yu D-G (2021) Electrospun medicated nanofibers for wound healing. Membranes (basel) 11:770. https://doi.org/10.3390/membranes11100770
Maddocks SE, Lopez MS, Rowlands RS, Cooper RA (2012) Manuka honey inhibits the development of Streptococcus pyogenes biofilms and causes reduced expression of two fibronectin binding proteins. Microbiology 158:781–790. https://doi.org/10.1099/mic.0.053959-0
Majtan J (2011) Methylglyoxal—a potential risk factor of manuka honey in healing of diabetic ulcers. Evid-Based Complement Altern Med. https://doi.org/10.1093/ecam/neq013
Maleki H, Gharehaghaji AA, Dijkstra PJ (2013) A novel honey-based nanofibrous scaffold for wound dressing application. J Appl Polym Sci 127:4086–4092. https://doi.org/10.1002/app.37601
Matica MA, Aachmann FL, Tøndervik A et al (2019) Chitosan as a wound dressing starting material: antimicrobial properties and mode of action. Int J Mol Sci 20:5889. https://doi.org/10.3390/ijms20235889
McDonald CM, Keeling SE, Brewer MJ, Hathaway SC (2018) Using chemical and DNA marker analysis to authenticate a high-value food, manuka honey. Npj Sci Food 2:1–14. https://doi.org/10.1038/s41538-018-0016-6
Molan P, Rhodes T (2015) Honey: a biologic wound dressing. Wounds 27:141–151
Moore OA, Smith LA, Campbell F et al (2001) Systematic review of the use of honey as a wound dressing. BMC Complement Altern Med 1:1–6
Morsi MA, Rajeh A, Menazea AA (2019) Nanosecond laser-irradiation assisted the improvement of structural, optical and thermal properties of polyvinyl pyrrolidone/carboxymethyl cellulose blend filled with gold nanoparticles. J Mater Sci Mater Electron 30:2693–2705. https://doi.org/10.1007/s10854-018-0545-4
Muktar MZ, Ismail WIW, Razak SIA et al (2018) Accelerated wound healing of physically cross linked gellan gum-virgin coconut oil hydrogel containing manuka honey. ASM Sci J 11:166–182
Nuutila K, Eriksson E (2021) Moist wound healing with commonly available dressings. Adv Wound Care 10:685–698. https://doi.org/10.1089/wound.2020.1232
Ozkizilcik A, Sharma A, Muresanu DF et al (2018) Timed release of cerebrolysin using drug-loaded titanate nanospheres reduces brain pathology and improves behavioral functions in Parkinson's disease. Mol Neurobiol 55:359–369. https://doi.org/10.1007/s12035-017-0747-4
Pan H, Wang W, Pan Y et al (2015) Construction of layer-by-layer assembled chitosan/titanate nanotubes based nanocoating on cotton fabrics: flame retardant performance and combustion behavior. Cellulose 22:911–923. https://doi.org/10.3390/ijms20235889
Pandey SK, Vishwakarma PK, Yadav SK et al (2019) Multi-walled carbon nanotube filters for toxin removal from cigarette smoke. ACS Appl Nano Mater 3:760–771. https://doi.org/10.1021/acsanm.9b02277
Parin FN, Terzioğlu P, Sicak Y et al (2021) Pine honey–loaded electrospun poly (vinyl alcohol)/gelatin nanofibers with antioxidant properties. J Text Inst 112:628–635. https://doi.org/10.1080/00405000.2020.1773199
Patel S, Cichello S (2013) Manuka honey: an emerging natural food with medicinal use. Nat Prod Bioprospect 3:121–128. https://doi.org/10.1007/s13659-013-0018-7
Pavan Kalyan BG, Kumar L (2022) 3D printing: applications in tissue engineering, medical devices, and drug delivery. AAPS PharmSciTech 23:1–20. https://doi.org/10.1208/s12249-022-02242-8
Payan A, Fattahi M, Jorfi S et al (2018) Synthesis and characterization of titanate nanotube/single-walled carbon nanotube (TNT/SWCNT) porous nanocomposite and its photocatalytic activity on 4-chlorophenol degradation under UV and solar irradiation. Appl Surf Sci 434:336–350. https://doi.org/10.1016/j.apsusc.2017.10.149
Pentoś K, Łuczycka D, Oszmiański J et al (2020) Polish honey as a source of antioxidants–a comparison with Manuka

honey. J Apic Res 59:939–945. https://doi.org/10.1080/00218839.2020.1723837
Rafter L, Reynolds TIM, Collier M et al (2017) A clinical evaluation of Algivon® Plus manuka honey dressings for chronic wounds. Wounds UK 13(4):80–140
Rajput A, Kulkarni M, Deshmukh P et al (2021) A key role by polymers in microneedle technology: a new era. Drug Dev Ind Pharm 47:1713–1732. https://doi.org/10.1080/03639045.2022.2058531
Ranjous Y, Regdon G Jr, Pintye-Hódi K, Sovány T (2019) Standpoint on the priority of TNTs and CNTs as targeted drug delivery systems. Drug Discov Today 24:1704–1709. https://doi.org/10.1016/j.drudis.2019.05.019
Razak SA, Mohd Gazzali A, Fisol FA et al (2021) Advances in nanocarriers for effective delivery of docetaxel in the treatment of lung cancer: an overview. Cancers (basel) 13:400. https://doi.org/10.3390/cancers13030400
Roberts AEL, Maddocks SE, Cooper RA (2012) Manuka honey is bactericidal against Pseudomonas aeruginosa and results in differential expression of oprF and algD. Microbiology 158:3005–3013. https://doi.org/10.1099/mic.0.062794-0
Ronsisvalle S, Lissandrello E, Fuochi V et al (2019) Antioxidant and antimicrobial properties of Casteanea sativa Miller chestnut honey produced on Mount Etna (Sicily). Nat Prod Res 33:843–850. https://doi.org/10.1080/14786419.2017.1413568
Sallem F, Boudon J, Heintz O et al (2017) Synthesis and characterization of chitosan-coated titanate nanotubes: towards a new safe nanocarrier. Dalt Trans 46:15386–15398. https://doi.org/10.1080/14786419.2017.1413568
Sandomierski M, Zielińska M, Buchwald T et al (2022) Controlled release of the drug for osteoporosis from the surface of titanium implants coated with calcium titanate. J Biomed Mater Res Part B Appl Biomater 110:431–437. https://doi.org/10.1002/jbm.b.34919
Sarhan WA, Azzazy HME, El-Sherbiny IM (2016) The effect of increasing honey concentration on the properties of the honey/polyvinyl alcohol/chitosan nanofibers. Mater Sci Eng C 67:276–284. https://doi.org/10.1016/j.msec.2016.05.006
Seidi F, Khodadadi Yazdi M, Jouyandeh M et al (2021) Chitosan-based blends for biomedical applications. Int J Biol Macromol 183:1818–1850. https://doi.org/10.1016/j.ijbiomac.2021.05.003
Shitole AA, Raut P, Giram P et al (2020) Poly (vinylpyrrolidone)-iodine engineered poly (ε-caprolactone) nanofibers as potential wound dressing materials. Mater Sci Eng C 110:110731. https://doi.org/10.1016/j.msec.2020.110731
Shoueir KR, El-Desouky N, Rashad MM et al (2021) Chitosan based-nanoparticles and nanocapsules: overview, physicochemical features, applications of a nanofibrous scaffold, and bioprinting. Int J Biol Macromol 167:1176–1197. https://doi.org/10.1016/j.ijbiomac.2020.11.072
Sinaei M, Heidari F, Hayati R (2020) Investigation of corrosion properties of nano-composite coatings of hydroxyapatite/barium titanate/chitosan produced by electrophoretic deposition on 316L stainless steel. Surf Eng Appl Electrochem 56:272–281. https://doi.org/10.3103/S1068375520030175
Sipos B, Pintye-Hódi K, Kónya Z et al (2017) Physicochemical characterisation and investigation of the bonding mechanisms of API-titanate nanotube composites as new drug carrier systems. Int J Pharm 518:119–129. https://doi.org/10.1016/j.ijpharm.2016.12.053
Siti Sarah MZ (2016) Potential protective effects of tualang honey and Ficus deltoidea dack var. deltoidea against bisphenol a induced toxicity in the reproductive system of pre-pubertal female rats/Siti Sarah Mohammad Zaid. https://doi.org/10.1016/j.ijpharm.2016.12.053
Stagos D, Soulitsiotis N, Tsadila C et al (2018) Antibacterial and antioxidant activity of different types of honey derived from Mount Olympus in Greece. Int J Mol Med 42:726–734. https://doi.org/10.3892/ijmm.2018.3656
Stevens MP, Haque A, Atkins T et al (2004) Attenuated virulence and protective efficacy of a Burkholderia pseudomallei bsa type III secretion mutant in murine models of melioidosis. Microbiology 150:2669–2676. https://doi.org/10.1099/mic.0.27146-0
Tang Y, Lan X, Liang C et al (2019) Honey loaded alginate/PVA nanofibrous membrane as potential bioactive wound dressing. Carbohyd Polym 219:113–120. https://doi.org/10.1016/j.carbpol.2019.05.004
Türkoğlu GC, Sarıışık AM, Karavana SY (2021) Development of textile-based sodium alginate and chitosan hydrogel dressings. Int J Polym Mater Polym Biomater 70:916–925. https://doi.org/10.1080/00914037.2020.1765364
Wang J, Sun J, Huang J et al (2021) Synthesis and its characterization of silver sulfide/nickel titanate/chitosan nanocomposites for photocatalysis and water splitting under visible light, and antibacterial studies. Mater Chem Phys 272:124990. https://doi.org/10.1016/j.matchemphys.2021.124990
Wani TU, Pandith AH, Sheikh FA (2021) Polyelectrolytic nature of chitosan: Influence on physicochemical properties and synthesis of nanoparticles. J Drug Deliv Sci Technol 65:102730. https://doi.org/10.1016/j.jddst.2021.102730
Xiao X, Zheng C, Cai S et al (2020) Optimization of nonlinear optical response of one-dimensional nanostructured sodium titanate through morphological control. NANO 15:2050086. https://doi.org/10.1142/S1793292020500861
Yilmaz AC, Aygin D (2020) Honey dressing in wound treatment: a systematic review. Complement Ther Med 51:102388. https://doi.org/10.1016/j.ctim.2020.102388
Zahedi P, Rezaeian I, Ranaei-Siadat S et al (2010) A review on wound dressings with an emphasis on electrospun nanofibrous polymeric bandages. Polym Adv Technol 21:77–95. https://doi.org/10.1002/pat.1625
Zidan HM, Abdelrazek EM, Abdelghany AM, Tarabiah AE (2019) Characterization and some physical studies of PVA/PVP filled with MWCNTs. J Mater Res Technol 8:904–913. https://doi.org/10.1016/j.jmrt.2018.04.023